ACS APPLIED NANO MATERIALS

www.acsanm.org Article

Proximity Effects of the Selective Atomic Layer Deposition of Cobalt on the Nanoscale: Implications for Interconnects

Michael Breeden, Victor Wang, Jacob Spiegelman, Ashay Anurag, Steven F. Wolf, Daniel Moser, Ravindra K. Kanjolia, Mansour Moinpour, Jacob Woodruff, Srinivas Nemani, Keith Wong, Charles H. Winter, and Andrew C. Kummel*

Cite This: *ACS Appl. Nano Mater.* 2021, 4, 8447−8454 Read Online

ACCESS | Metrics & More | Article Recommendations | Supporting Information

ABSTRACT: The continued scaling of transistor sizes has motivated the need to replace Cu with alternate metals to minimize resistivity, with cobalt being of interest for both interconnect via metallization as well as emerging die-bonding processes. The atomic layer deposition of cobalt using $Co(tBu_2DAD)_2$ and tertiary-butyl amine has nearly infinite selectivity (>1000 cycles) on metallic vs insulating (SiO_2 or low-k SiCOH dielectric) planar samples. However, on patterned samples, selectivity under identical atomic layer deposition (ALD) conditions is limited, due to the diffusion of molecularly adsorbed metal precursors from reactive to non-reactive surfaces. X-ray photoelectron spectroscopy (XPS) and scanning electron microscopy (SEM) were employed to investigate the effects of process parameters on surface precursor diffusion to determine the mechanism of selectivity loss on the nanoscale. Top-down SEM and XPS spectra of a striped test pattern of Cu and SiO_2 indicated that selective vapor-phase passivation of SiO_2 improved the selectivity for deposition on Cu versus SiO_2 by reducing the number of insulator defects that facilitated trapping of precursor molecules and subsequent Co nucleus growth. The remaining nuclei were present due to incomplete defect passivation. Conversely, near-perfect selectivity during Co ALD was obtained with the periodic annealing of the substrate, consistent with a low temperature reflow process, allowing for Co nuclei on SiO_2 defects to merge with the metallic growth surface.

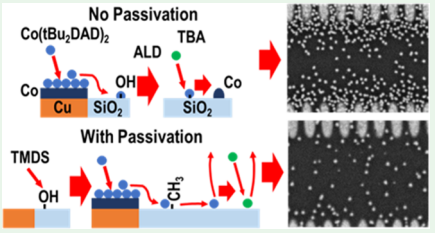

KEYWORDS: *cobalt, atomic layer deposition (ALD), area-selective ALD, X-ray photoelectron spectroscopy (XPS), interconnect metallization*

INTRODUCTION

With continued scaling of transistors to smaller nodes, the increasing resistivity of Cu interconnects deposited by electrodeposition in middle-of-line (MOL) and back-end-of-line (BEOL) processing motivates the search for alternate interconnect metals and deposition techniques at the M0/M1 interconnect layers.[1,2] One such metal is Co, which has been shown to be effective as a Cu capping layer to protect Cu from oxidation and as a Cu replacement in tightly confined vias where electroplating Cu is more difficult.[3,4] Atomic layer deposition (ALD) is an effective method to deposit Co due to its controllability of thickness and conformality over high-aspect ratio structures. In addition, different surface chemistries can be exploited to allow for area-selective deposition, enabling bottom-up fill on metals.[5] Bottom-up fill in interconnect vias has previously been explored as a means of avoiding void formation during ALD of metals[6] but is also hypothesized to encourage vertical grain growth, thereby limiting the effects of grain boundary scattering. Another novel application of such a selective Co ALD process is in the bonding of suspended Cu pads to form electrical contacts, enabling tighter-packed connections between bonded dies during packaging.[7] Selective ALD of the Co metal has previously been reported using several precursors such as $Co(AMD)_2$ and (^{t}Bu-Allyl)$Co(CO)_3$.[8,9] Of special interest is one selective Co ALD process reported by the Winter group using bis(1,4-di*tert*-butyl-1,3-diazadienyl) cobalt [$Co(tBu_2DAD)_2$] and formic acid at 180 C, exhibiting a very high selectivity toward metals versus insulators.[10,11] Additional studies on the deposition of Co using $Co(tBu_2DAD)_2$ were performed using *tert*-butylamine to avoid oxidation of metallic substrates.[12,13]

During area-selective ALD on conductors versus insulators, loss of selectivity can result from surface defects (such as hydroxyl groups) on insulators causing unwanted nucleation.[14] This problem is magnified by close proximity to the desired growth surface, where it is hypothesized that excess precursors remaining weakly bound to the growth surface may diffuse onto the insulator. The diffused precursor may then bind with surface defects and subsequently react with the ALD coreactant (e.g., a metal precursor reacting with a reducing

Received: June 30, 2021
Accepted: July 16, 2021
Published: July 30, 2021

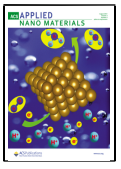

Downloaded via UNIV OF CALIFORNIA SAN DIEGO on August 28, 2022 at 23:10:42 (UTC).
See https://pubs.acs.org/sharingguidelines for options on how to legitimately share published articles.

© 2021 American Chemical Society

https://doi.org/10.1021/acsanm.1c01639
ACS Appl. Nano Mater. 2021, 4, 8447−8454

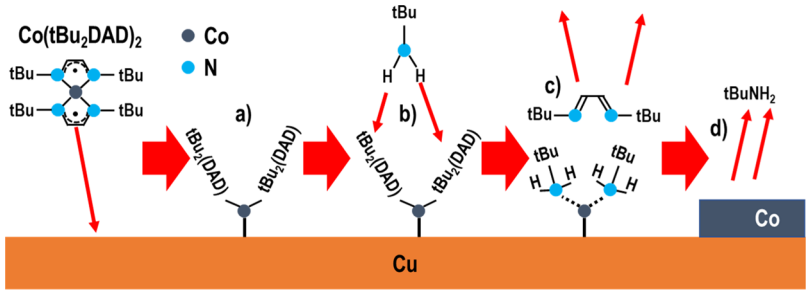

Figure 1. Mechanism of Co(tBu$_2$DAD)$_2$ + TBA ALD 180 °C. (a) During the Co(tBu$_2$DAD)$_2$ cycle, Co(tBu$_2$DAD)$_2$ chemisorbs to the metal surface, leaving two tBu$_2$(DAD) ligands bound to Co on surface. (b) During the TBA half-cycle, tBuNH$_2$ exchanges with tBu$_2$(DAD) ligands. (c) tBu$_2$(DAD) ligands desorb from surface, leaving behind metal surface with the N atom in tBuNH$_2$ coordinated to Co metal. (d) tBuNH$_2$ subsequently desorbs from the surface, leaving behind Co metal.

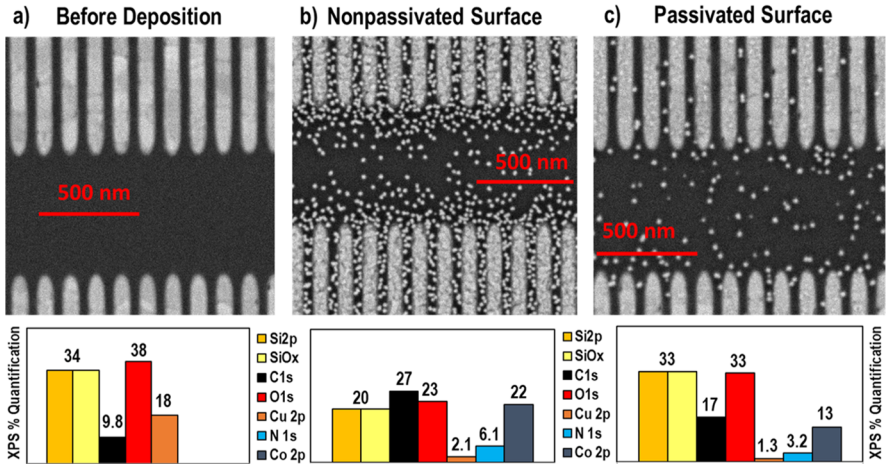

Figure 2. Two hundred cycles of Co(DAD)$_2$ + TBA at 180 °C on a patterned Cu/SiO$_2$ structure. (a) Top-down SEM of Cu/SiO$_2$ pattern showing ~85 nm wide Cu (light gray) stripes deposited planar to SiO$_2$ (dark gray) prior to deposition of Co by ALD. Before deposition, 18% Cu and 34% Si are observed by XPS. (b) After 200 cycles (with 8x pulses of Co and 5 s pump-out times) on the unpassivated sample, unwanted Co nuclei are observed close to the Co/Cu stripes. XPS quantification shows 22% Co and 20% Si on the unpassivated surface, suggesting significant coverage of unwanted nuclei attenuating the Si signal. (c) On a passivated sample, the density of unwanted nuclei is 4x lower and more uniform. XPS quantification shows 13% Co, with 33% Si signal, consistent with less Co coverage over the passivated SiO$_2$ surface.

agent) in the next ALD half-cycle to form nuclei for subsequent growth.[15] Grillo et al. argue that the surface diffusion of excess metal precursors on insulator surfaces can lead to the formation of nanoparticle nuclei which can serve as points for unwanted nucleation on insulators.[16,17] Hydroxyl groups present on SiO$_2$-based insulators which serve as binding sites for precursors can be deactivated through the use of Si-based vapor-phase passivants prior to deposition, thereby enhancing area-selectivity during metal ALD.[18] This study seeks to understand the mechanism by which unwanted Co nuclei appear on insulators within a few nanometers of the metallic growth surface and compares optimization techniques to improve selectivity and determine the atomistic mechanisms of selectivity enhancement. *In-situ* X-ray photoelectron spectroscopy (XPS) and *ex-situ* SEM are used to characterize the loss of selectivity during Co deposition on nanoscale test strips of alternating Cu/SiO$_2$ surfaces. SEM and transmission electron microscopy (TEM) illustrate that periodic anneals induce a low temperature reflow of these nanoscale nuclei, thereby greatly improving selectivity on the nanoscale.

EXPERIMENTAL METHODOLOGY

In this report, Co ALD was performed using the coreactants Co(tBu$_2$DAD)$_2$ (EMD Performance Materials, Inc.) and TBA at 180 °C on a test pattern consisting of Cu stripes embedded in SiO$_2$.[12,13] In this process, the Co(tBu$_2$DAD)$_2$ precursor bound to the Cu metal surface engages in ligand exchange with the dosed TBA to form Co metal plus amine ligands, which are subsequently desorbed during pump-down as described in eq 1 and Figure 1.

$$\text{Co half-cycle: } \text{Co}(t\text{Bu}_2\text{DAD})_2(\text{g}) + \text{Co(s)} \rightarrow \text{Co}(t\text{Bu}_2\text{DAD})_2(\text{ad})$$

$$\text{TBA half-cycle: } \text{Co}(t\text{Bu}_2\text{DAD})_2\,(\text{ad}) + 2t\text{BuNH}_2\,(\text{g}) \rightarrow (t\text{BuNH}_2)_2\text{Co}\,(\text{ad}) + 2(t\text{Bu}_2\text{DAD})\,(\text{g})$$

$$\text{desorption step: } (t\text{BuNH}_2)_2\text{Co}\,(\text{ad}) \rightarrow \text{Co}\,(\text{s}) + 2t\text{BuNH}_2\,(\text{g})$$

$$\text{half-cycle reactions for Co(DAD)}_2 + \text{TBA Co ALD process} \quad (1)$$

Figure 2a is a top-down SEM image (see the full image in Figure S1 in Supporting Information) of the test pattern prior to Co ALD, consisting of 85 nm wide strips of Cu deposited via electrodeposition on a TiN/Si substrate, then planarized by chemical−mechanical polishing (CMP). A degrease and 0.5% HF clean were performed on the post-CMP samples to minimize surface contamination. Prior to deposition, all samples were cleaned with acetone, methanol, and water rinses, followed by a final 30 s 0.5% HF dip prior to being mounted on a sample holder and loaded into the load lock of the deposition and analysis chamber. The analysis chamber (Figure S2 in Supporting Information) consists of a load-lock, deposition chamber

https://doi.org/10.1021/acsanm.1c01639
ACS Appl. Nano Mater. 2021, 4, 8447−8454

for ALD, and UHV chamber (~10^{-10} Torr base pressure) containing the X-ray source and analyzer for XPS. Once loaded, samples were first transferred into the UHV chamber for a 30 min 350 °C vacuum anneal using a pyrolytic boron nitride heater to remove residual airborne carbon contaminants and leave a clean starting substrate. The deposition chamber and dosing lines were pumped with a turbomolecular pump (Pfeiffer TMP-151C) with a base pressure of 10^{-6} Torr, and the wall temperature was maintained at 125 °C. The sample stage was heated to 180 °C through an enclosed cartridge heater inside a Cu block welded to a high-vacuum flange to eliminate the possibility of hot-wire CVD reactions. The turbomolecular pump was used to pump away precursor gases between pulses to avoid any possible O_2 contamination from purge gas and to prevent any parasitic CVD component that might lead to undesired nucleation. The Co(tBu$_2$DAD)$_2$ precursor bottle temperature was 120 °C, and the dosing lines were maintained at a temperature range of 10−20 °C higher to avoid condensation of precursor in lines. Ultrahigh purity N_2 was passed through a purifier before being sent through the precursor bottle at 1 Torr to act as a carrier gas for delivery to the deposition chamber. The Co(tBu$_2$DAD)$_2$ precursor bottle was refilled with a carrier gas for 200 ms, followed by a 200 ms pulse into the ALD reactor at a pressure of ~200 mTorr, which is repeated for each pulse of the precursor. To achieve the required precursor dose, multiple pulses of precursor per half-cycle were employed, as the compression ratio of the turbomolecular pump drops drastically above the mTorr range, limiting the pumping speed. The co-reactant *tert*-butylamine (Me_3CNH_2, TBA, Sigma-Aldrich) was maintained at 25 °C and dosed in 20 ms pulses to limit pressure spikes to 1 Torr. No purge gas was used between half-cycles to limit potential oxygen incorporation in the deposited Co, with the pump-out time of precursor varying as a process parameter. The resulting ALD sequence was a Co(tBu$_2$DAD)$_2$ dose followed by pump-out, a dose of TBA, and ending with a 20 s pump-out.

After deposition, the samples were transferred *in situ* to the UHV chamber for XPS. A monochromatic XM1000 MkII/SPHERA system (Omicron Nanotechnology GmbH) was used to collect XPS spectra with an Al kα source at 1486.7 eV, with an analyzer pass energy of 50 eV and a linewidth of 0.1 eV. XPS spectra were collected at 60° with respect to the sample surface normal. XPS quantification was performed using CASA XPS 2.3 software, with raw peak areas corrected via Schofield photoionization cross-sectional relative sensitivity factors. Due to the presence of an uncompensated sample charging during XPS, the location of the Si 2p peak was used to establish the charge shift in XPS spectra based on the known Si 2p peak location for SiO_2 of 103 eV per sample, and applied to the Co 2p3/2 peak to verify the presence of Co metal. Top-down SEM was also performed after Co ALD using a FEI Apreo scanning electron microscope at 2 kV electron voltage and 0.05 nA emission current using a backscatter electron detector. Finally, cross-sectional TEM of the Cu/SiO_2 striped patterns was performed.

RESULTS AND DISCUSSION

The Co(tBu$_2$DAD)$_2$ + TBA ALD process was employed on patterned substrates with Cu lines separated by SiO_2 (Figures 2a, S1 in Supporting Information). In Figure 2b (Figure S3 in Supporting Information), XPS quantification shows significant attenuation of both Cu and Si signals from 18% to 2.1% Cu coverage and 34−20% Si coverage compared with the pre-deposition surface. SEM imaging shows the presence of a significant amount of Co nuclei on the SiO_2, with the density being highest near the Cu and decreasing with distance from the stripes. In addition, nearly all of the nuclei are of a similar diameter, with 95% of particles being between 230−298 nm^2 with oblong disc shapes as observed in SEM and TEM imagery. From the work of Wolf et al., it is observed that selectivity on un-patterned SiO_2 during Co ALD with Co(tBu$_2$DAD)$_2$ is consistent with the lack of molecular adsorption.[12] Nuclei 2−4 nm tall are observed by AFM on blanket SiO_2, but it is hypothesized that there are more hydroxyl groups on patterned SiO_2 due to defects formed during CMP of the surface compared with thermally grown SiO_2, so that the proximity of the Co/Cu surfaces is more likely to result in unwanted adsorption of Co precursor on the hydroxyl groups and therefore, unwanted nucleation.

To confirm this hypothesis, a Cu/SiO_2 patterned sample was passivated with vapor-phase dimethylamino-dimethyl-silazane ($(Me_2N)_2SiMe_2$, DMADMS) and tetramethyl-disilazane [$(Me_2SiH)_2NH$, TMDS] in a 50% mixture of both species at 5 Torr for 10 min at 70 °C, followed by deposition of 200 Co ALD cycles. TMDS and DMADMS are commonly used for SiCOH repair, as they readily bind to hydroxyl groups formed via plasma damage during dry etching.[19] Simultaneous vapor-phase dosing of both TMDS and DMADMS was employed to silylate both isolated and geminal hydroxyl groups on SiO_2.[20] Figure 2c (Figure S4 in Supporting Information) shows the SEM of the passivated SiO_2/Cu striped surface after Co ALD. On the passivated surface, XPS quantification (raw XPS spectra shown as Figure S9 before deposition, S10 after deposition without passivation, and S7 after deposition with passivation in Supporting Information) shown in the bottom of Figure 2c after 200 ALD cycles shows only 13% Co and 33% Si, similar to the clean surface and therefore consistent with lower Co coverage on the SiO_2. To determine the chemical state of the Co layer deposited, the chemical shift of the Co2p peak was measured. On both the unpassivated and the passivated samples, the peak location of the Co2p3/2 peak after correction for uncompensated sample charging was centered at 778 eV, consistent with metallic Co formation (see Figures S10 and S11 in Supporting Information for peak shifts and charge correction factors).

SEM imaging in Figure 2b,c shows a high density of Co nuclei on the unpassivated SiO_2, with a far lower density on the passivated SiO_2, consistent with the XPS data. Unlike the unpassivated sample, however, the distribution of Co nuclei on the insulator is far more evenly distributed. For any unwanted nuclei formed on the unpassivated insulator surface in the initial ALD cycles, it is hypothesized that subsequent cycles will see these nuclei act as adsorption sites in subsequent cycles. Because the number of defect sites on SiO_2 is expected to be a fixed number throughout the process, nucleation should occur within the first few cycles for most sites, resulting in further growth leading to nuclei of a similar size. The nuclei density on the passivated SiO_2, however, is expected to be lower due to the presence of fewer defect sites, with remaining nuclei being present due to incompletely passivated hydroxyl groups. These SEM and XPS observations, therefore, are consistent with unwanted nuclei being formed by diffusion of the Co(tBu$_2$DAD)$_2$ precursor from the Cu strip to a fixed number of defects on the SiO_2, where it is trapped and converted to Co with subsequent TBA pulses. The fixed number of defects can be reduced by vapor-phase passivation of hydroxyl groups, resulting in a lower density of Co nuclei.

As mentioned, the presence of unwanted nuclei on the unpassivated insulator is significantly greater than that of the unpassivated insulator. To quantify the density of unwanted nuclei on the insulator, the image analysis software ImageJ was used to identify and sort nuclei as a function of distance from the stripe edges.[21] Figure 3 illustrates the difference in unwanted nucleation density with a histogram of the number of nuclei as a function of distance from the top striped pattern in the 600 nm wide insulator alley. On the unpassivated Cu/

https://doi.org/10.1021/acsanm.1c01639
ACS Appl. Nano Mater. 2021, 4, 8447−8454

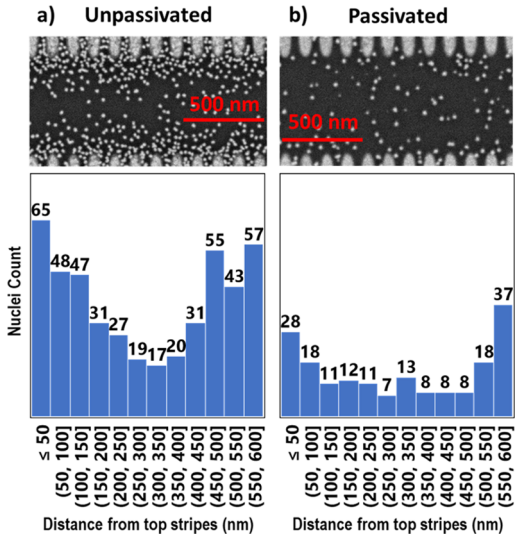

Figure 3. SEM and nuclei distance distribution from stripes on passivated vs unpassivated Cu/SiO_2 pattern after Co ALD. Co is light gray and SiO_2 dark gray in the SEM images above. Below, nuclei counts are plotted in bins of 50 nm. (a) After 200 cycles on the unpassivated sample, there is a decay in nuclei density until the middle of the alley. (b) On a passivated sample, the density of unwanted nuclei is lower and more uniform across SiO_2.

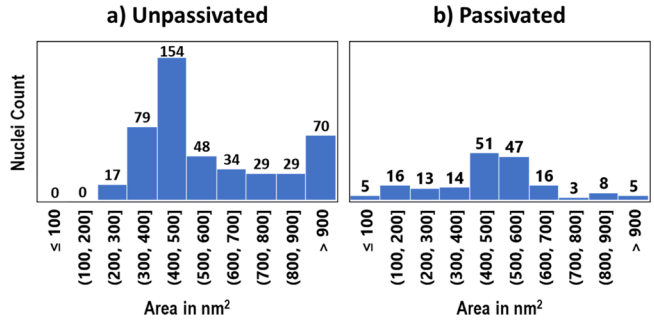

Figure 4. Nucleus size distribution on passivated vs unpassivated Cu/SiO_2 striped pattern after Co ALD. Nuclei areas are plotted in bins of 50 nm^2. (a) Unpassivated surface and (b) passivated surface.

SiO_2 pattern (Figure 3a), there is a gradual drop off in the nuclei density with the distance from the top edge of the striped pattern to the middle of the alley with an overall nuclei coverage of 19% and density of 294 nuclei/μm^2. On the passivated sample (Figure 3b), a decrease in nuclei count to a density of 114 nuclei/μm^2 and an overall coverage overall coverage of 5% is observed, with a near-constant nuclei density across the insulator. As the pump-out time between cycles is on the order of seconds, precursor molecules should have sufficient time to diffuse or desorb off the insulator surface before the co-reactant can react to form a nucleus, leaving the defect density on the insulator as the limiting factor in nuclei density. With the passivated surface, the defect density is reduced by the presence of fewer hydroxyl groups, further limiting the number of sites where a nucleus can be formed. This result, therefore, is consistent with passivation offering $Co(tBu_2DAD)_2$ physisorbed on the insulator fewer sites to be trapped on before diffusing back to the growth surface or desorbing entirely. Future work in the numerical modeling of surface diffusion in area-selective ALD, therefore, should account for the presence of defects that trap excess precursor to capture this effect.

Figure 4 (full histograms in Figures S5 and S6 for unpassivated and passivate surfaces, respectively) illustrates the nuclei size distribution on the insulator surface. The mean nucleus size on the passivated surface is 458 nm^2, with a standard deviation of 181 nm^2 and skewness of −0.22. On the unpassivated sample, the average nucleus size is 503 nm^2 with a standard deviation of 155 nm^2 and skewness of 0.83. Given the model of surface diffusion onto insulator defects, it is expected that mean nuclei sizes will be larger on the passivated surface due to the presence of fewer total sites for a given flux of excess precursor. However, a smaller mean nuclei size is observed on the passivated surface with a negatively skewed distribution, contrary to this model. One possible explanation for this is that delayed nucleation on marginally passivated sites occurs later during deposition, resulting in smaller nuclei at those sites. On the unpassivated surface, the distribution is positively skewed, with many larger nuclei observed. One possibility is that two nuclei in close proximity grow together to form a single large nucleus during growth. The second possibility is an artifact of the finite sharpness of the SEM images, resulting in two (or more) close nuclei falsely appearing as a single larger nucleus. Due to the far higher nuclei density on the unpassivated surface, the positive skewness of the nuclei size distribution is consistent with a combination of these two factors.

The small insulator areas in between the Cu stripes were also examined for undesired nuclei. As the area of the insulator is comparable to the area of the Cu fingers, precursor molecules are equally likely to land on an insulator as they are on metals. Once precursors trapped by insulator defects form initial nuclei, further cycles may result in precursors directly adsorbing on these nuclei, with the growing nuclei likely to form an undesired bridge between the Cu lines. Quantification in this region was again performed using the abovementioned method. Any detected nuclei overlapping the Cu stripes were discarded from the count, as well as nuclei touching the edge of the image in order to get a consistent count of nuclei sizes. Figure 5a is a top-down SEM image of the striped portion of the Cu/SiO_2 pattern without passivation along with a histogram of the nuclei size distribution (Figure S3 in Supporting Information, full histogram in Figure S7), while 5b is the same portion with passivation (Figure S4 in Supporting Information, full histogram in Figure S8). The distribution of nucleus sizes on the passivated sample is centered around a mean value of 496 nm^2 with a standard deviation of 123 nm^2 and skewness of 0.62, while on the unpassivated sample, a similar distribution with a mean nuclei size of 470 nm^2, standard distribution of 185 nm^2, and skewness of 0.60 is observed. Although the nuclei density is far lower for the passivated surface, the size distribution of nuclei on both surfaces is similarly skewed upward, with the unpassivated surface having a longer tail of sizes reflecting the greater presence of multiple nuclei in proximity being counted as one. The presence of larger particles on average after passivation is consistent with a lower defect density allowing for the precursor to more readily diffuse and re-absorb onto the metal strips, with the remaining nuclei being able to capture more excess precursors.

While the possibility that Cu contamination on the insulator during the CMP process is the source of Co nucleation was considered, if Cu contamination was the driving force behind undesired nucleation, the spatial distribution of nuclei should remain unchanged after passivation; however, the observed

https://doi.org/10.1021/acsanm.1c01639
ACS Appl. Nano Mater. 2021, 4, 8447−8454

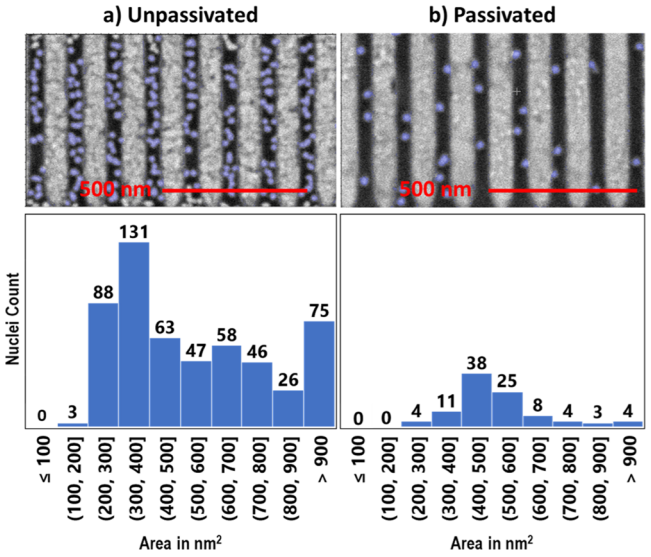

Figure 5. Two hundred cycles of Co(tBu$_2$DAD)$_2$ + TBA at 180 °C (8× Co pulses, 5 s pump-out) on a patterned Cu/SiO$_2$ sample—nuclei quantification in close proximity to growth surface. The Cu stripes are gray, and the SiO$_2$ areas are black. (a) Without passivation, 186 nuclei/μm^2 are observed with an average size of 470 nm^2 and positively skewed distribution. (b) With passivation, 33 nuclei/μm^2 are observed with a similar distribution centered around a larger mean nucleus size.

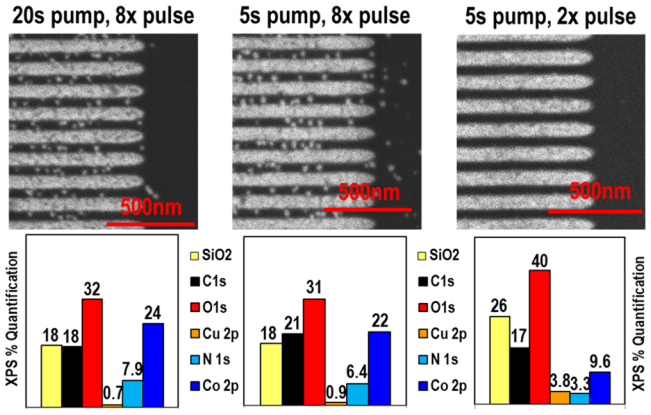

Figure 6. Two hundred cycles of Co(tBu$_2$DAD)$_2$ + TBA at 180 °C on a patterned Cu/SiO$_2$ sample without insulator passivation. The Cu stripes are gray, and the SiO$_2$ areas are black. Increasing pump-out time has a strong effect on nuclei density in the large open SiO$_2$ areas but a weak effect on nucleation density on the narrow SiO$_2$ regions between the metal strips. The dose of Co(tBu$_2$DAD)$_2$ in each cycle was then reduced by 4×, with near perfect selectivity with 2× pulse and half the growth rate. Raw SEM images and XPS spectra of the above samples are included in Supporting Information as Figs. S13 and S17 for the 8× Co pulse/20 s pump-out time condition; S12 and S16 for the 8× Co pulse/5 s pump-out time condition; and S18 and S20 for the 2× Co pulse/5 s pump-out time condition, respectively.

distribution is consistent with defect sites primarily being hydroxyl groups, not Cu contaminant sites. These results, therefore, confirm the hypothesis that the loss of selectivity on the nanoscale is due to surface precursor diffusion to defects. With a higher sticking probability, metal surfaces will experience a precursor saturation before the insulator surface, resulting in a concentration gradient that can drive diffusion and cause unwanted growth.

The Co(tBu$_2$DAD)$_2$ + TBA ALD is unusual because XPS data are consistent with molecular chemisorption instead of dissociative chemisorption of Co(tBu$_2$DAD)$_2$ at 180 °C; previous XPS studies with this precursor show that the tBu$_2$DAD ligands are largely intact after the surface is dosed with Co(tBu$_2$DAD)$_2$.[12] This implies that the Co(tBu$_2$DAD)$_2$ adsorption is reversible; therefore, it was hypothesized that selectivity could also be improved by increasing the pump-out time so that Co(tBu$_2$DAD)$_2$ which diffused onto the SiO$_2$ could desorb before the subsequent TBA pulse reacted with the tBu$_2$DAD ligands from Co(tBu$_2$DAD)$_2$ to induce irreversible adsorption. To study the effect of these process parameters on nucleation density, pump-out time and dose amount were varied without the use of a passivant. As shown in Figure 6 (SEM images Figures S12 and S13, cross-sectional TEM Figures S14 and S15, respectively, in Supporting Information), increasing the pump-out time from 5 s to 20 s decreased the density of unwanted nuclei, consistent with the Co(tBu$_2$DAD)$_2$ diffusion and the reversible adsorption hypotheses. As with the passivation comparison, nuclei density on the insulator surface away from the edges of the stripes was quantified, with a decrease from 52 to 9 nuclei/μm^2 when the pump-out time is increased. However, inspecting the narrow insulator stripes between adjacent Cu stripes shows relatively little decrease in nucleation density, and XPS quantification (raw XPS spectra, Figures S16 and S17 in Supporting Information, respectively) shows a negligible difference in the surface coverage of Co versus Cu.

The Co(tBu$_2$DAD)$_2$ likely initially adsorbs strongly to the Co metallic growth surface, but during each ALD cycle, excess Co(tBu$_2$DAD)$_2$ is employed to ensure saturation on the growth surface as illustrated in Figure 7a. Therefore, at the end

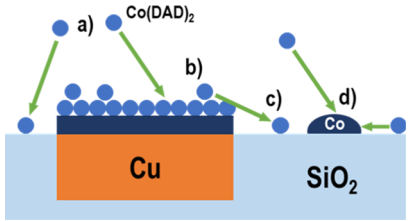

Figure 7. Mechanism of excess Co(tBu$_2$DAD)$_2$ precursor surface diffusion onto an insulator. (a) Dosing of the Co(tBu$_2$DAD)$_2$ precursor onto both metal and insulator surfaces, with precursor binding to metal while only physisorbing on the insulator. (b) Saturated metal surface with excess precursors being weakly bound to surface and free to diffuse. (c) Diffusion of excess precursors off the saturated metal surface onto the insulator. (d) Co nuclei formed on the insulator defects; excess precursors diffusing across the insulator will bind with the nucleus in addition to dosed precursor.

of each Co(tBu$_2$DAD)$_2$ pulse, weakly adsorbed Co(tBu$_2$DAD)$_2$ is present on the metal surface, as illustrated in Figure 7b. It was hypothesized that during each ALD cycle, once the growth surface was saturated with Co(tBu$_2$DAD)$_2$, further dosing would result in this weakly adsorbed precursor to diffuse onto the SiO$_2$ (Figure 7c). This excess precursor can diffuse across the SiO$_2$ until it reaches a surface hydroxyl or a pre-existing Co defect nucleus to react (Figure 7d) or desorb. To test this hypothesis, a lower Co(tBu$_2$DAD)$_2$ dose was employed by reducing the number of pulses per cycle. As shown by SEM in Figure 6 (Figures S13 and S18 in Supporting Information), this was very effective in reducing the number of

https://doi.org/10.1021/acsanm.1c01639
ACS Appl. Nano Mater. 2021, 4, 8447−8454

unwanted nuclei on the SiO_2, with zero observed nuclei on the insulator surface, but the growth rate was significantly reduced. XPS quantification of the 8× and 2× pulse conditions shows a factor of 2 reduction in Co surface coverage as seen in the XPS quantification in Figure 6, and lower Cu attenuation, consistent with a lower growth rate. To confirm this growth rate decrease, thickness was estimated by TEM in Figures S14 and S19 in Supporting Information. The average thickness of the Co film deposited with the 8× pulse condition was determined to be 15 nm, while the average thickness under the 2× pulse condition was 7.6 nm, a factor of 2 reduction.

Cross-sectional TEM was performed as shown in Figure 8 to further illustrate the effects of pump time and dose process

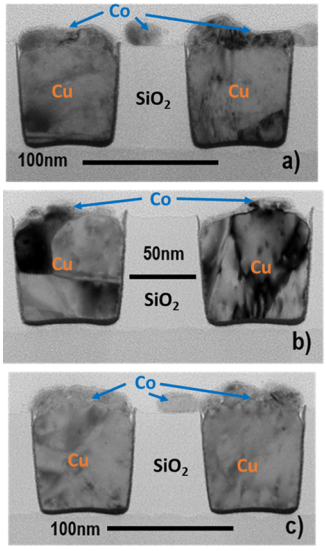

Figure 8. TEM of 200 Co ALD cycles with varying pump-out time and dose without passivation. The Cu stripes are dark gray, and the SiO_2 areas are white. (a) With 8 pulses of Co precursor per cycle, and 5 s pump-out time, unwanted nucleation density is high. (b) Reducing Co pulse count to 2 pulses/cycle with 5 s pump-out time lowers the growth rate. (c) Increasing the pump-out time from 5 s to 20 s for 8 pulses of Co precursor per cycle improves unwanted nucleation density, but higher precursor does not eliminate unwanted nucleation.

parameters absent passivation. In Figure 8a (full image included in Supporting Information as Figure S14), unwanted nucleation density on the Cu/SiO_2 strip pattern is high, consistent with the top-down SEM results. In Figure 8b (full image included Supporting Information as Figure S19), reduced Co dosing resulted in a thinner layer of Co on Cu, consistent with a lower growth rate as confirmed by XPS studies (see Figure S24 in Supporting Information for raw XPS spectra). In Figure 8c (full image included in Supporting Information as Figure S15), the increased pump-out time reduces but does not eliminate, unwanted nucleation.

Current Co CVD fill processes for interconnect vias use reflow to ensure a void-free via fills. During Co CVD growth, the Co film layer grows inward until the via closes up, leaving behind a void. To eliminate this void, annealing is performed at roughly 350−400 °C to reflow the Co metal to fully fill the via.[22] Another method hypothesized to improve selectivity is to introduce a periodic anneal step in between sets of cycles to act as a mid-deposition reflow. According to the simple Ostwald ripening model, atoms from small nuclei can more readily diffuse than atoms from large nuclei; therefore, by annealing the surface periodically during deposition while nuclei are smaller, it may be possible to induce Co diffusion from the nuclei to the Co/Cu stripes at a lower temperature than a typical reflow process. To test this hypothesis, after each 100 Co ALD cycles, annealing to 260 °C for 30 min in ultrahigh vacuum was performed, which is around 140 °C below the normal Co reflow temperature.[22−24] As the temperature of Co ALD is far below the anneal temperature and cycle times are on the order of 50× shorter than the anneal time, diffusion of Co nuclei is expected to be negligible during growth, necessitating the periodic anneal step.

TEM cross sections of the Cu/SiO_2 fingers along with XPS quantification are shown in Figure 9 for both nonannealed and

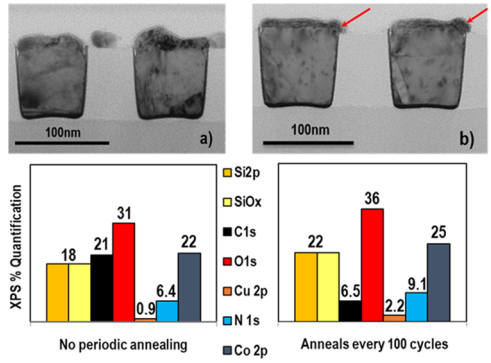

Figure 9. TEM and XPS of 200 cycles of $Co(tBu_2DAD)_2$ + TBA at 180 °C on a patterned Cu/SiO_2 sample with 260 °C periodic anneal after each 100 ALD cycles. TEM of the Cu stripes after deposition with Cu in dark gray and SiO_2 in light gray. Co ALD was performed on an unpassivated surface. Eight pulses of Co precursor were dosed per Co half-cycle, followed by a 5 s pump-out. (a) Without periodic anneal, unwanted nucleation is observed on SiO_2, with the Si signal in XPS being more attenuated than on the annealed sample. (b) After periodic anneals every 100 cycles, a denser film is observed, with the formation of bulges at stripe edges (red arrow) consistent with nanoscale reflow of Co. The periodically annealed surface exhibited near-perfect selectivity, with no observed nuclei on the insulator (SEM images in Supporting Information Figures S22 and S23, respectively).

annealed samples. TEM (full images available in Supporting Information as Figures S14 and S21, respectively) shows that without periodic anneals (Figure 9a), nuclei are observed on the insulator in addition to the Cu stripes. On the annealed sample in Figure 9b, however, the formation of a bulge (seen using the red arrow) at the edges of the stripes is observed. Furthermore, SEM imagery of the nonannealed and annealed samples (Supporting Information Figures S22 and S23, respectively) shows that periodically annealing the sample every 100 cycles completely prevented the formation of nuclei on the insulator. XPS of the nonannealed and annealed samples (full XPS spectra of each element available in Supporting Information as Figures S16 and S24, respectively), likewise, shows less insulator attenuation and greater Co signal on the annealed sample than on the nonannealed sample, which is consistent with near-perfect selectivity on the Cu/SiO_2 pattern without the use of passivation. This observation is consistent with the reflow of Co nuclei below a critical diameter on the SiO_2 to the edges of the Cu growth surface, forming an edge bulge as it binds to the existing Co metal layer. As the temperature of this anneal is 140 °C lower than that of typical reflow processes, this has the potential to further

https://doi.org/10.1021/acsanm.1c01639
ACS Appl. Nano Mater. 2021, 4, 8447−8454

scale the thickness of the diffusion barrier between the Co and the SiCOH. An alternative to the periodic anneal process while exploiting this reflow effect would be a hypothetical higher-temperature selective ALD process for Co where dissociation occurs only on metal surfaces at temperatures around 250−300 °C to continually reflow during deposition and prevent nuclei from forming on insulator. Selective Co ALD processes have been reported around 350 °C, but require the use of a self-assembled monolayer to block deposition on the undesired growth region first.[25] Periodically annealing allows for the high selectivity of passivated area-selective ALD, while avoiding the need for a long blocking layer which may limit the usefulness of Co in highly confined interconnect vias.

CONCLUSIONS

The proximity effect of unwanted nucleation of metals on insulators by excess precursors during selective-area ALD of Co is demonstrated using the precursor $Co(tBu_2DAD)_2$ with *tert*-butyl amine as a co-reactant. Four strategies have been found to improve Co ALD selectivity: adding a passivant to remove insulator defect sites, increasing the pump-out time, decreasing the precursor dose, and periodic annealing. The periodic annealing technique allows for reabsorption of the Co nuclei from the insulator surface to the growth surface and is consistent with a low temperature reflow process. The strategies of passivation and periodically annealing the film to avoid Co nuclei are of great importance when considering integration of selective Co deposition by ALD in tightly confined patterns for interconnects, as well as emerging applications in the bonding of suspended Cu pads for die−die bonding in IC packaging.

ASSOCIATED CONTENT

Supporting Information

The Supporting Information is available free of charge at https://pubs.acs.org/doi/10.1021/acsanm.1c01639.

SEM image of Cu/SiO_2 pattern before deposition, chamber schematic of combined ALD and XPS analysis chamber, SEM images of Cu/SiO_2 pattern after 200 cycles Co ALD without passivation, nuclei counts as counted by ImageJ for unpassivated surface on insulator away from Cu stripes, nuclei count as counted by ImageJ for passivated surface on insulator between Cu stripes, XPS Spectra of Cu/SiO_2 pattern before deposition and after 30 min, XPS Spectra of Cu/SiO_2 pattern after 200 cycles Co ALD without passivation, TEM image of Cu/SiO_2 pattern after 200 cycles Co ALD, and XPS Spectra of Cu/SiO_2 pattern after 200 cycles Co ALD at various pulse and pump-out values (PDF)

AUTHOR INFORMATION

Corresponding Author

Andrew C. Kummel − *Department of Chemistry and Biochemistry, University of California, La Jolla, California 92093, United States;* orcid.org/0000-0001-8301-9855; Email: akummel@ucsd.edu

Authors

Michael Breeden − *Materials Science and Engineering Program, University of California, La Jolla, California 92093, United States*

Victor Wang − *Materials Science and Engineering Program, University of California, La Jolla, California 92093, United States*

Jacob Spiegelman − *Materials Science and Engineering Program, University of California, La Jolla, California 92093, United States*

Ashay Anurag − *Materials Science and Engineering Program, University of California, La Jolla, California 92093, United States*

Steven F. Wolf − *Materials Science and Engineering Program, University of California, La Jolla, California 92093, United States*

Daniel Moser − *EMD Performance Materials, Haverhill, Massachusetts 01831, United States*

Ravindra K. Kanjolia − *EMD Performance Materials, Haverhill, Massachusetts 01831, United States*

Mansour Moinpour − *EMD Performance Materials, Haverhill, Massachusetts 01831, United States*

Jacob Woodruff − *EMD Performance Materials, Haverhill, Massachusetts 01831, United States*

Srinivas Nemani − *Applied Materials, Sunnyvale, California 95054, United States*

Keith Wong − *Applied Materials, Sunnyvale, California 95054, United States*

Charles H. Winter − *Department of Chemistry, Wayne State University, Detroit, Michigan 48202, United States;* orcid.org/0000-0003-0416-1234

Complete contact information is available at: https://pubs.acs.org/10.1021/acsanm.1c01639

Notes

The authors declare no competing financial interest.

ACKNOWLEDGMENTS

This work was supported in part by the Applications and Systems-Driven Center for Energy Efficient Integrated Nano Technologies (ASCENT), one of six centers in the Joint University Microelectronics Program (JUMP), an SRC program sponsored by the Defense Advanced Research Program Agency (DARPA). The authors would also like to gratefully acknowledge support from Applied Materials. This work was also performed in part at the San Diego Nanotechnology Infrastructure (SDNI) of UCSD, a member of the National Nanotechnology Coordinated Infrastructure, which is supported by the National Science Foundation (grant ECCS-1542148).

REFERENCES

(1) Gall, D. The search for the most conductive metal for narrow interconnect lines. *J. Appl. Phys.* **2020**, *127*, 050901.

(2) Plombon, J. J.; Andideh, E.; Dubin, V. M.; Maiz, J. Influence of phonon, geometry, impurity, and grain size on Copper line resistivity. *Appl. Phys. Lett.* **2006**, *89*, 113124.

(3) Yang, C.-C.; Flaitz, P.; Wang, P.-C.; Chen, F.; Edelstein, D. Characterization of selectively deposited cobalt capping layers: Selectivity and electromigration resistance. *IEEE Electron Device Lett.* **2010**, *31*, 728−730.

(4) Carpio, R.; Jaworski, A. Review-Management of Copper Damascene Plating. *J. Electrochem. Soc.* **2019**, *166*, D3072−D3096.

(5) Parsons, G. N.; Clark, R. D. Area-Selective Deposition: Fundamentals, Applications, and Future Outlook. *Chem. Mater.* **2020**, *32*, 4920−4953.

(6) Zyulkov, I.; Krishtab, M.; De Gendt, S.; Armini, S. Selective Ru ALD as a Catalyst for Sub-Seven-Nanometer Bottom-Up Metal Interconnects. *ACS Appl. Mater. Interfaces* **2017**, *9*, 31031−31041.
(7) Li, M.-J.; Breeden, M.; Wang, V.; Hollin, J.; Linn, N. M. K.; Winter, C. H.; Kummel, A.; Bakir, M. S. Cu-Cu Bonding Using Selective Cobalt Atomic Layer Deposition for 2.5-D/3-D Chip Integration Technologies. *IEEE Trans. Compon., Packag., Manuf. Technol.* **2020**, *10*, 2125−2128.
(8) Elko-Hansen, T. D.-M.; Ekerdt, J. G. Selective Atomic Layer Deposition of Cobalt for Back End of Line. *ECS Trans.* **2017**, *80*, 29−37.
(9) Kwon, J.; Saly, M.; Halls, M. D.; Kanjolia, R. K.; Chabal, Y. J. Substrate Selectivity of (^{t}Bu-Allyl)Co(CO)$_3$ during Thermal Atomic Layer Deposition of Cobalt. *Chem. Mater.* **2012**, *24*, 1025−1030.
(10) Klesko, J. P.; Kerrigan, M. M.; Winter, C. H. Low Temperature Thermal Atomic Layer Deposition of Cobalt Metal Films. *Chem. Mater.* **2016**, *28*, 700−703.
(11) Kerrigan, M. M.; Klesko, J. P.; Rupich, S. M.; Dezelah, C. L.; Kanjolia, R. K.; Chabal, Y. J.; Winter, C. H. Substrate selectivity in the low temperature atomic layer deposition of cobalt metal films from bis(1,4-di-tert-butyl-1,3-diazadienyl)cobalt and formic acid. *J. Chem. Phys.* **2017**, *146*, 052813.
(12) Wolf, S.; Breeden, M.; Ueda, S.; Woodruff, J.; Moinpour, M.; Kanjolla, R.; Kummel, A. C. The role of oxide formation on insulating versus metallic substrates during Co and Ru selective ALD. *Appl. Surf. Sci.* **2019**, *510*, 144804.
(13) Kerrigan, M. M.; Klesko, J. P.; Winter, C. H. Low Temperature, Selective Atomic Layer Deposition of Cobalt Metal Films Using Bis(1,4-di-tert-butyl-1,3-diazadienyl)cobalt and Alkylamine Precursors. *Chem. Mater.* **2017**, *29*, 7458−7466.
(14) Lee, H.-B.-R.; Kim, W.-H.; Lee, J. W.; Kim, J.; Hwang, I. The degradation of deposition blocking layer during area selective plasma enhanced atomic layer deposition of cobalt. *J. Korean Phys. Soc.* **2010**, *1*, 104−107.
(15) Mackus, A. J. M.; Merkx, M. J. M.; Kessels, W. M. M. From the Bottom-up: Toward Area-Selective Atomic Layer Deposition with High Selectivity. *Chem. Mater.* **2019**, *31*, 2−12.
(16) Soethoudt, J.; Grillo, F.; Marques, E. A.; van Ommen, J. R.; Tomczak, Y.; Nyns, L.; Elshocht, S. V.; Delabie, A. Diffusion-mediated growth and size-dependent nanoparticle reactivity during ruthenium atomic layer deposition on dielectric substrates. *Adv. Mater. Interfaces* **2018**, *5*, 1800870.
(17) Grillo, F.; Moulijn, J. A.; Kreutzer, M. T.; van Ommen, J. R. Nanoparticle sintering in atomic layer deposition of supported catalysts: Kinetic modeling of the size distribution. *Catal. Today* **2018**, *316*, 51−61.
(18) Khan, R.; Shong, B.; Ko, B. G.; Lee, J. K.; Lee, H.; Park, J. Y.; Oh, I.-K.; Raya, S. S.; Hong, H. M.; Chung, K.-B.; Luber, E. J.; Kim, Y.-S.; Lee, C.-H.; Kim, W.-H.; Lee, H.-B. -R. Area-selective atomic layer deposition using Si precursors as inhibitors. *Chem. Mater.* **2018**, *30*, 7603−7610.
(19) Imada, T.; Nakata, Y.; Ozaki, S.; Kobayashi, Y.; Nakamura, T. Systematic investigation of silylation materials for recovery use of low-kmaterial plasma damage. *Jpn. J. Appl. Phys.* **2015**, *54*, 071502.
(20) Sneh, O.; George, S. M. Thermal Stability of Hydroxyl Groups on a Well-Defined Silica Surface. *J. Phys. Chem.* **1995**, *99*, 4639−4647.
(21) Abramoff, M. D.; Magalhaes, P. J.; Ram, S. J. Image processing with ImageJ. *Biophot. Int.* **2004**, *11*, 36−42.
(22) Kokaze, Y.; Kodaira, S.; Endo, Y.; Hamaguchi, J.; Harada, M.; Kumamoto, S.; Sakamoto, Y.; Higuchi, Y. Performance of Integrated Cu Gap-Filling Process with Chemical Vapor Deposition Cobalt Liner. *Jpn. J. Appl. Phys.* **2013**, *52*, 05FA01.
(23) Kim, H.; Kamineni, V.; Sung, M. G.; Park, C. Low line resistivity and repeatable metal recess using CVD cobalt reflow. U.S. Patent 9,362,377 B1 filed 02-27, 2015.
(24) Nogami, T.; Patlolla, R.; Kelly, J.; Briggs, B.; Huang, H.; Demarest, J.; Li, J.; Hengstebeck, R.; Zhang, X.; Lian, G.; Peethala, B.; Bhosale, P.; Maniscalco, J.; Shobha, H.; Nguyen, S.; McLaughlin, P.; Standaert, T.; Canaperi, D.; Edelstein, D.; Paruchuri, V. Cobalt/copper composite interconnects for line resistance reduction in both fine and wide lines. *2017 IEEE International Interconnect Technology Conference (IITC). Hsinchu, Taiwan*, 2017; pp 1−3.
(25) Lee, H.-B. -R.; Kim, W.-H.; Lee, J. W.; Kim, J.-M.; Heo, K.; Hwang, I. C.; Park, Y.; Hong, S.; Kim, H. High Quality Area-Selective Atomic Layer Deposition Co Using Ammonia Gas as a Reactant. *J. Electrochem. Soc.* **2010**, *157*, D10.

https://doi.org/10.1021/acsanm.1c01639
ACS Appl. Nano Mater. 2021, 4, 8447−8454